On the wavenumber spectra for sound within subsonic jets

A. Agarwal[a)]
Department of Engineering, University of Cambridge, Trumpington Street, Cambridge CB2 1PZ, United Kingdom

S. Sinayoko and R. D. Sandberg
Faculty of Engineering and the Environment, University of Southampton, Highfield, Southampton SO17 1BJ, United Kingdom

(Received 16 January 2014; revised 27 June 2014; accepted 8 July 2014)

This paper explores the nature of sound spectra within subsonic jets. Three problems of increasing complexity are presented. First, a point source is placed in a two-dimensional plug flow and the sound field is obtained analytically. Second, a point source is embedded in a diverging axisymmetric jet and the sound field is obtained by solving the linearized Euler equations. Finally, an analysis of the acoustic waves propagating through a turbulent jet obtained by direct numerical simulation is presented. In each problem, the pressure or density field is analyzed in the frequency-wavenumber domain. It is found that acoustic waves can be classified into three main frequency-dependent groups. A physical justification is provided for this classification. The main conclusion is that, at low Strouhal numbers, acoustic waves satisfy the d'Alembertian dispersion relation. © *2014 Acoustical Society of America*. [http://dx.doi.org/10.1121/1.4890648]

PACS number(s): 43.28.Py, 43.28.Ra, 43.60.Lq [AH] Pages: 1029–1035

I. INTRODUCTION

Our initial motivation for understanding the sound spectra in jets came from the article by Goldstein (2005) in which he proposed that it may be possible to identify the "true" sources of noise in jets if the radiating and non-radiating components could be separated. It is possible to achieve this separation for the Euler equations linearized about either a steady uniform base flow (Chu and Kovasznay, 1958) or a steady parallel flow (Agarwal *et al.*, 2004). Unfortunately, existing separation techniques cannot be applied to full non-linear Navier-Stokes equations and, hence, are not useful for realistic jets.

Sinayoko *et al.* (2011) showed that filtering in the frequency-wavenumber domain is an effective technique for separating radiating and non-radiating components in subsonic jets. Their filtering technique relied on the dispersion relation, $k = |\omega|/c_\infty$ (where k denotes the magnitude of the wavenumber, ω is the angular frequency, and c_∞ is the far field speed of sound) satisfied by acoustic waves radiating to a quiescent far field. But, inside the jet, we can have waves that travel supersonically, relative to the ambient medium. In this paper, we define acoustic waves in jets as those satisfying the dispersion relation, $k_z \leq |\omega|/c_\infty$, where k_z denotes the axial wavenumber. In other words, in the axial direction, acoustic waves travel either upstream ($k_z \leq 0$) or downstream ($0 \leq k_z \leq |\omega|/c_\infty$); in the downstream case, the axial phase speed is, therefore, sonic or supersonic. The characterization of acoustic waves by supersonic axial phase speed was used by Freund (2001), Cabana *et al.* (2008), Tinney and Jordan (2008), and Obrist (2009). The results presented in this paper support this definition of acoustic waves.

The filtering technique is represented diagrammatically in Fig. 1. The radiating part, $q'(\boldsymbol{x}, t)$, of a flow field variable, $q(\boldsymbol{x}, t)$, can be obtained by convolving q with an appropriate filter function, $w(\boldsymbol{x}, t)$, which is defined in the frequency-wavenumber domain $[W(\boldsymbol{k}, \omega)]$. Sinayoko *et al.* (2011) considered a model problem in which the base flow corresponding to the experiment of the Mach 0.9, Re 3600 jet by Stromberg *et al.* (1980) was excited by two instability waves at nondimensional frequencies of 2.2 and 3.4. These waves interact nonlinearly to produce acoustic waves at the difference frequency of 1.2. The density field at frequency 1.2 is shown in Fig. 2(a). In this problem, both acoustic and hydrodynamic waves are being generated. The Fourier transform of this field, $P(\boldsymbol{k}, \omega)$, is shown in Fig. 2(b). Multiplying $P(\boldsymbol{k}, \omega)$ with $W(\boldsymbol{k}, \omega)$, as defined in Fig. 1, gives $P'(\boldsymbol{k}, \omega)$, which is shown in Fig. 2(d). The Fourier transform of the remaining field, $\bar{P}(\boldsymbol{k}, \omega) = P - P'$, is shown in Fig. 2(f). The corresponding density fields in the space-time domain are obtained by applying the inverse Fourier transforms and are shown in Figs. 2(c) and 2(e). Radiating components have captured all the acoustic waves. Clearly, the acoustic waves have been separated from the hydrodynamic waves. However, the efficacy of the filter is puzzling as it is based on the dispersion relation for sound propagation in a uniform quiescent medium. Inside the jet, we do not have a quiescent medium, so how can this dispersion relation separate acoustic waves both outside and inside the jet?

In order to answer this question, we have constructed a simple model problem for sound radiation from a point source in a two-dimensional plug flow (Sec. II). We show that, for this problem, it is possible to obtain an analytical expression for the Fourier transform for both the axial and cross-stream directions. This is a crucial step in obtaining the spectral characteristics of sound propagation and it enables us to understand and explain the observed acoustic

a)Author to whom correspondence should be addressed. Electronic mail: aa406@cam.ac.uk

Redistribution subject to ASA license or copyright; see http://acousticalsociety.org/content/terms. Download to IP: 152.78.242.156 On: Wed, 17 Dec 2014 10:07:03

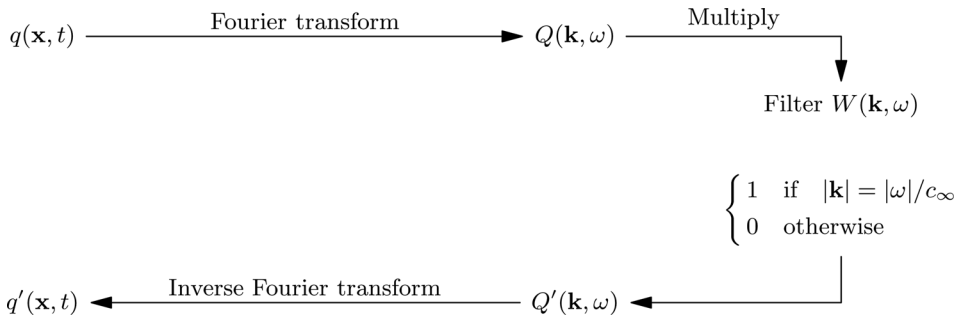

FIG. 1. Algorithm for filtering out the radiating field. For numerical implementation, $W(\boldsymbol{k},\omega)$ has a finite width (see Sinayoko *et al.*, 2011 for details).

wavenumber spectra for different frequencies. The solution to this problem also indicates how to identify acoustic waves for more general (turbulent) jets. In Sec. III, we consider a more general problem of sound radiation from a point source in a diverging cylindrical jet and in Sec. IV we identify the acoustic waves using data obtained from a direct numerical simulation (DNS) of a Mach 0.84, Re 7200 turbulent jet.

Even though our motivation for identifying acoustic waves in turbulent jets stems from a particular application, as mentioned above, this work can be used in other ways. For example, the flow filtering technique defined here could be used to separate convecting and propagating components in a jet. This can help define various source models or correlate the near field hydrodynamic data to the acoustic far field to identify the noise producing regions in the jet. The technique can also be used to correctly identify the radiating part of Lighthill's source term (Freund, 2001; Cabana *et al.*, 2008; Sinayoko and Agarwal, 2012).

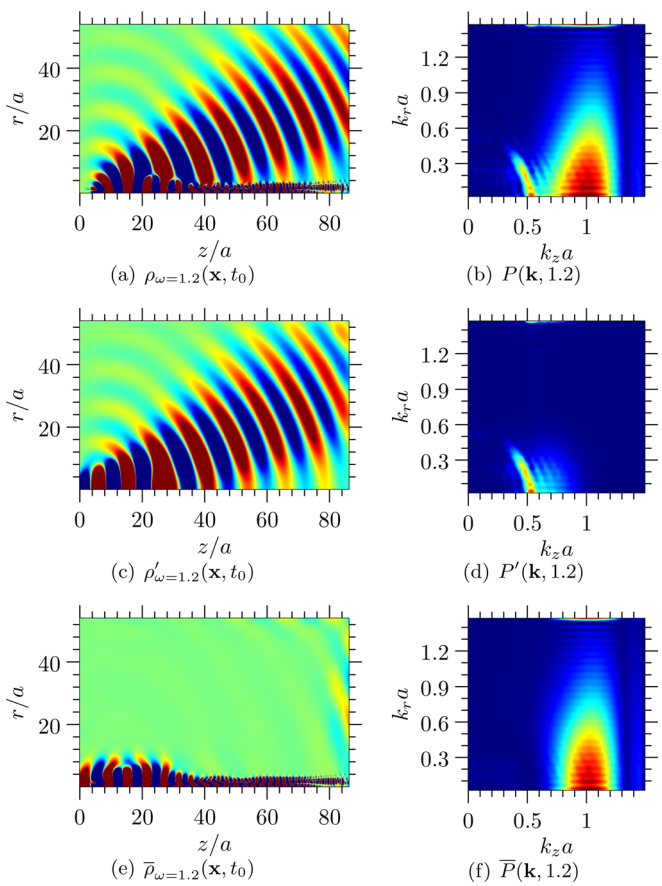

FIG. 2. (Color online) Density field in a turbulent jet of exit radius, a, plotted in the physical domain (snapshot in left column) and wavenumber domain (magnitude of Fourier transform in right column) with color range $[-5\times10^{-5}, 5\times10^{-5}]$ and $[0, 0.5]$, respectively, for a given normalized frequency, $\omega = 1.2$ and time, t_0 [cf. Eq. (19)]. The top row shows the density field, ρ, the middle row shows the radiating field, ρ', and the bottom row shows the non-radiating field, $\bar{\rho}$.

II. MODEL PROBLEM

Consider the problem of a time-harmonic monopole point mass source, $\rho_o\delta(\boldsymbol{x})\exp(-i\omega t)$ (ρ_o denotes ambient density), embedded in a plug flow. Several authors (e.g., Morgan, 1975; Mani, 1972) have considered the problem of far field sound radiation from a point source in axisymmetric jets. The main difference between their analysis and ours is that we seek the spectral content in the frequency-wavenumber domain instead of the far field characteristics of sound in the physical domain.

For simplicity, we consider a two-dimensional problem. The problem setup is described in Fig. 3. Assuming an $\exp(-i\omega t)$ response [$\phi(\boldsymbol{x},t) = \phi(\boldsymbol{x};w)\exp(-i\omega t)$], the linear velocity potential, ϕ_I, for small disturbances satisfies, in region I (outside the jet),

$$\nabla^2\phi_I + \kappa^2\phi_I = 0, \tag{1}$$

and in region II, inside the jet,

$$\nabla^2\phi_{II} - \left(-i\kappa + M\frac{\partial}{\partial x}\right)^2\phi_{II} = \delta(x)\delta(y), \tag{2}$$

where ∇^2 denotes the Laplacian operator, $\kappa = \omega/c$ is the acoustic wavenumber, and c is the speed of sound, which is uniform for the present problem. Because the velocity potential and pressure are symmetric about the mid-plane axis of

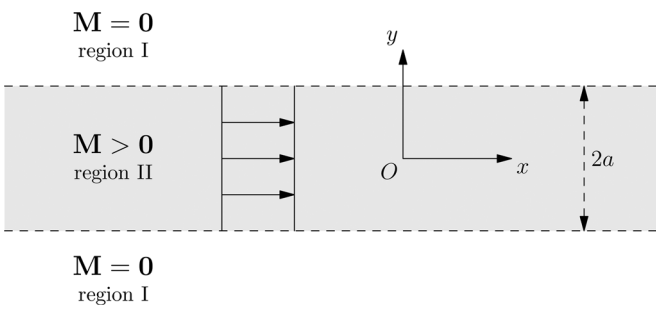

FIG. 3. Schematic sketch of a point source located at the origin inside a two-dimensional plug flow of width $2a$. The flow Mach number is $M > 0$ for $|y| < a$ (region II) and $M = 0$, otherwise (region I).

Redistribution subject to ASA license or copyright; see http://acousticalsociety.org/content/terms. Download to IP: 152.78.242.156 On: Wed, 17 Dec 2014 10:07:03

the jet ($y = 0$), it is sufficient to solve the problem for $y \geq 0$. Continuity of pressure at $y = a$ requires that $p = -\rho_o D\phi/Dt$ be continuous (D/Dt denotes material derivative), therefore,

$$\left(-i\kappa + M\frac{\partial}{\partial x}\right)\phi_{II}(x,a) = -i\kappa\phi_I(x,a). \tag{3}$$

The kinematic constraint requires that particle displacement, η, at the interface be continuous. Therefore,

$$\frac{\partial}{\partial y}\phi_I(x,a) = \frac{\partial}{\partial t}\eta(x,a), \tag{4}$$

$$\frac{\partial}{\partial y}\phi_{II}(x,a) = \frac{\partial}{\partial t}\eta(x,a) + Mc\frac{\partial}{\partial x}\eta(x,a). \tag{5}$$

Applying the Fourier transform in x, defined by

$$\hat{\phi}(k_x) = \int_{-\infty}^{\infty}\phi(x)e^{-ik_x x}dx, \tag{6}$$

to Eqs. (1) and (2), we get

$$\frac{d^2\hat{\phi}_I}{dy^2} + \left(\kappa^2 - k_x^2\right)\hat{\phi}_I = 0, \tag{7}$$

$$\frac{d^2\hat{\phi}_{II}}{dy^2} + \left((\kappa - k_x M)^2 - k_x^2\right)\hat{\phi}_{II} = \delta(y). \tag{8}$$

Application of the Fourier transform in the axial direction to Eqs. (3)–(5) gives

$$(\kappa - k_x M)\hat{\phi}_{II}(k_x,a) = \kappa\hat{\phi}_I(k_x,a), \tag{9}$$

$$\kappa\frac{d\hat{\phi}_{II}}{dy}(k_x,a) = (\kappa - k_x M)\frac{d\hat{\phi}_I}{dy}(k_x,a). \tag{10}$$

Let $\beta^2 = \kappa^2 - k_x^2$ and $\gamma^2 = (\kappa - k_x M)^2 - k_x^2$. The location of the branch cuts for β and γ are shown in Fig. 4. The branch of the square roots are chosen such that both β and γ are equal to κ for $k_x = 0$. Acoustic waves propagate to the far field only when β is real, i.e., when $|k_x| < \kappa$. Therefore, we will focus on this range of wavenumbers. In region I, for outgoing waves to infinity,

$$\hat{\phi}_I = Ae^{i\beta y}. \tag{11}$$

Taking into account the symmetry about the mid-plane axis, the solution in region II is given by

$$\hat{\phi}_{II} = 2B\cos(\gamma y) - \frac{i}{2}\frac{e^{i\gamma y}}{\gamma}. \tag{12}$$

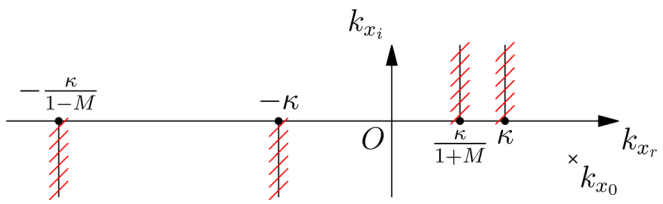

FIG. 4. (Color online) Location of the branch cuts for β and γ (hatched lines) and the Kelvin-Helmholtz instability pole, k_{x0}, in the complex k_x domain.

Application of conditions (9) and (10) yields

$$A = -\frac{i\kappa\exp(-ia\beta)(\kappa - Mk_x)}{2\Delta(\kappa,k_x,\gamma)}, \tag{13}$$

$$B = \frac{\exp(ia\gamma)\left(\kappa^2\gamma - \beta(\kappa - Mk_x)^2\right)}{4\gamma i\Delta(\kappa,k_x,\gamma)}, \tag{14}$$

where $\Delta(\kappa,k_x,k_y) = \beta\cos(ak_y)(\kappa - Mk_x)^2 - i\kappa^2 k_y\sin(ak_y)$. Note that for $M = 0$, we recover the free-field Green's function of the Helmholtz equation.

Equation $\Delta(\kappa,k_x,\gamma) = 0$ is the dispersion relation for the hydrodynamic wave. The roots of this equation represent poles of $\hat{\phi}$ in the complex k_x domain. For the present problem, there is one root, k_{x0}, which is located in the lower-half k_x-plane and is associated with a Kelvin-Helmholtz instability wave; it is purely hydrodynamic (Agarwal *et al.*, 2004) and does not affect our analysis. If our problem had a pipe (or two splitter plates in two dimensions) the Kelvin-Helmholtz instability wave would have an amplitude given by the edge condition, usually an unsteady Kutta condition [see, for example, Crighton (1985)]. Again, the Kelvin-Helmholtz wave would be subsonic and, hence, would not interfere with our analysis.

Defining the Fourier transform in y by

$$\hat{\hat{\phi}}(k_x,k_y) = \int_{-\infty}^{\infty}\hat{\phi}(k_x,y)e^{-ik_y y}\,dy, \tag{15}$$

the Fourier transform of the pressure field can be written as

$$\hat{\hat{p}}(k_x,k_y) = -2i\rho_o\int_0^{\infty}[\kappa\hat{\phi}_{II}(k_x,y)H(a-y) + (\kappa - k_x M)\hat{\phi}_I(k_x,y)H(y-a)]\cos(k_y y)\,dy. \tag{16}$$

This integral can be evaluated analytically

$$\hat{\hat{p}}(k_x,k_y) = \frac{\rho_o(\kappa - Mk_x)}{\Delta(\kappa,k_x,\gamma)}\left[\frac{i\left(\Delta(\kappa,k_x,k_y) - \Delta(\kappa,k_x,\gamma)\right)}{k_y^2 - \gamma^2} + \frac{\kappa^2\left(k_y\sin(ak_y) + i\beta\cos(ak_y)\right)}{k_y^2 - \beta^2}\right]. \tag{17}$$

A. Frequency-wavenumber spectra

The acoustic-wave solution in the physical domain can be obtained by applying the inverse Fourier transforms to Eq. (17) (for details on the geometry of the Fourier integration contours, F_x and F_y, and the implications on causality, see Agarwal *et al.*, 2004)

$$p(x,y;\omega) = \int_{F_x}\frac{dk_x}{2\pi}e^{ik_x x}\int_{F_y}\frac{dk_y}{2\pi}e^{ik_y y}\hat{\hat{p}}(k_x,k_y). \tag{18}$$

If we look at the k_y integral, because of the presence of $\hat{\hat{p}}(k_x,k_y)$ [see Eq. (17)], it has two terms. The second term has poles at $k_y = \pm\beta$. Using the method of residues, it can be shown that only these poles contribute to the integral. Therefore,

Redistribution subject to ASA license or copyright; see http://acousticalsociety.org/content/terms. Download to IP: 152.78.242.156 On: Wed, 17 Dec 2014 10:07:03

regardless of the frequency, only the wavenumbers that satisfy the dispersion relation $k_x^2 + k_y^2 = \kappa^2$ contribute to the integral. We refer to this as the radiation circle. The other term in the integrand has zeroes in the denominator at $k_y = \pm\gamma$, which corresponds to an ellipse in the wavenumber domain. Note that these zeroes do not represent poles as the numerator also goes to zero at $k_y = \pm\gamma$. Therefore, the contribution from the integrand is more complicated for this term. Further insight can be obtained by plotting the integrand as a function of frequency. Recall that $\kappa = \omega/c$ and from hereon, for brevity, the reduced frequency, κa, is referred to as frequency.

Figure 5 shows the wavenumber spectra, $|\hat{\hat{p}}(k_x, k_y)|$, for $M = 0.9$ for four different frequencies. At low frequencies $(\kappa a \ll 1)$, most of the energy is concentrated around the radiation circle [Fig. 5(a)]. For higher frequencies $[\kappa a = O(1)]$, the energy is concentrated along the radiation circle as well, but there is a small amount of energy around the vertical line, $k_x = \kappa/(1+M)$ [Figs. 5(b) and 5(c)]. For very high frequencies $(\kappa a \gg 1)$, we see the radiation circle and a part of the ellipse, $k_y^2 = \gamma^2$ [Fig. 5(d)]. We observe some ringing around the ellipse.

For jet noise, another useful nondimensional frequency is the Strouhal number, St, based on the jet diameter and exit velocity. It can be shown that $\mathrm{St} = \kappa a/(\pi M)$. High-speed jet noise peaks at $\mathrm{St} \sim 0.2$ $(\kappa a = 0.2M\pi)$. This suggests that for filtering out acoustic waves in a jet, around the peak radiation frequency, one need not worry about the ellipse in Fig. 5(d). For sound radiation near the peak frequency, the dispersion characteristics are very similar to those of the ordinary wave equation. This explains why Sinayoko *et al.* (2011) obtained a good separation of acoustic and hydrodynamic fields by using a filter based on the dispersion characteristics of the ordinary wave equation.

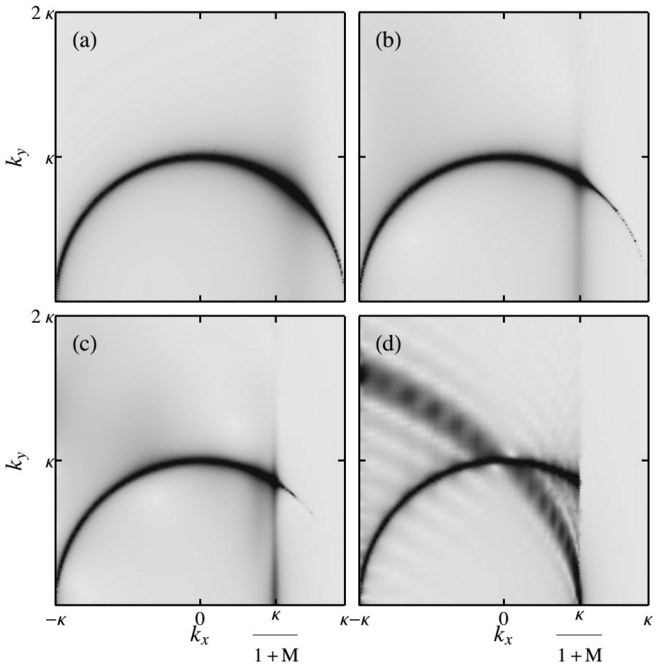

FIG. 5. Wavenumber spectra of the pressure field, $|\hat{\hat{p}}|$, from a point source in a jet (setup of Fig. 3) at frequency (a) $\kappa a = 0.1\pi$, (b) $\kappa a = \pi$, (c) $\kappa a = 2\pi$, (d) $\kappa a = 10\pi$. The density plot uses a linear scale from 0 (white) to $10\pi/\kappa$ (black).

1. Low frequencies

A mathematical justification for this low-frequency result can be obtained as follows. Assume $\kappa a \ll 1$. For acoustic waves, the wavenumbers, k_x and k_y, which satisfy the dispersion relation, are of the same order of magnitude as κ, so that $\gamma a \ll 1$ and $k_y a \ll 1$. In Eq. (17), if we expand the trigonometric functions in a power series up to the second order, it simplifies to

$$\hat{\hat{p}}(k_x, k_y) \approx \frac{\rho_o \beta(\kappa - Mk_x)[\kappa^2(i - a\beta) + O((a\kappa)^4)]}{\Delta(\kappa, k_x, \gamma)(k_y^2 - \beta^2)}.$$

From this equation, it is clear that at low frequencies the dispersion relation for the problem is $k_y^2 - \beta^2 = 0$, i.e., $k_x^2 + k_y^2 = (\omega/c)^2$, which is the dispersion relation for sound propagation through a uniform medium at rest. This indicates that mean flow has a negligible effect on sound propagation at low frequencies. This has been observed experimentally by Cavalieri *et al.* (2012).

The results can be interpreted by considering the potential field, $\hat{\phi}(k_x, y)$, given by Eqs. (11) and (12). Figure 6(a) shows the associated pressure field, $\hat{p}(k_x, y)$, as a function of y for $k_x = \kappa/(1+M)$ for two different values of κa, 0.1π, and π.

For $k_x = \kappa/(1+M)$, $\gamma = 0$ and, from Eq. (12), it is clear that $\hat{p}$ does not have a wave-like solution for $y \le a$. For brevity, we consider only the real part of $\hat{p}$, which can be shown to be a constant with respect to y in the limit $\gamma \to 0$. For $y > a$, the response is given by the harmonic function, $\exp(i\beta y)$. At low frequencies (e.g., $\kappa a = 0.1\pi$), the constant part (when $y < a$) is a very small part of a wavelength [Fig. 6(a)] and, therefore, when we Fourier transform this field, most of the energy is concentrated around $k_y = \pm\beta$. A similar argument applies to other values of k_x. Therefore, the presence of the jet has a negligible effect on the wavenumber spectrum at low frequencies.

2. Mid-range frequencies

As the frequency increases, the region in the y-domain over which the pressure field is a constant [when $k_x = \kappa/(1+M)$] occupies a larger part of the wavelength [see the dashed line in Fig. 6(a)]. This has a significant impact on the Fourier transform (in y) of $\hat{p}$. Instead of being concentrated just around $k_y = \pm\beta$, the energy in the k_y space gets distributed over a range of k_y values. The same

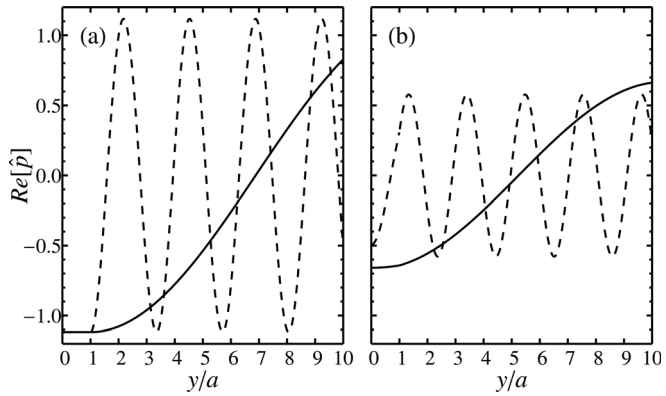

FIG. 6. Comparison of the pressure field, $\hat{p}(k_x, y)$, at $\kappa a = 0.1\pi$ (solid line) and $\kappa a = \pi$ (dashed line) for (a) $k_x = \kappa/(1+M)$ and (b) $k_x = 0.5\kappa/(1+M)$.

Redistribution subject to ASA license or copyright; see http://acousticalsociety.org/content/terms. Download to IP: 152.78.242.156 On: Wed, 17 Dec 2014 10:07:03

reasoning applies to other values of k_x close to $\kappa/(1+M)$. This explains the vertical patch in the spectra around $k_x = \kappa/(1+M)$ in Figs. 5(b) and 5(c).

Away from these values, in the range $0 < k_x < \kappa/(1+M)$, unless the frequency is very high, the pressure field inside the jet is very similar to that outside the jet. This is illustrated in Fig. 6(b), which shows the pressure field, $\hat{p}(k_x, y)$, for $k_x = 0.5\kappa/(1+M)$, for $\kappa a = 0.1\pi$ (solid line), and $\kappa a = \pi$ (dashed line). Therefore, for $0 < k_x < \kappa/(1+M)$, the Fourier transform of the pressure field is concentrated around the radiation circle, $k_y = \pm\beta$.

The energy in the k_y direction appears to be contained mainly inside the radiation circle around $k_x = \kappa/(1+M)$. This can be explained as follows. The difference between the constant field for $y < a$ and the sinusoid, $\exp(i\beta y)$, which would exist in the absence of a jet, is related to the Heaviside function, $H(a-y)$. The Fourier transform of this function is given by the sinc function, $\mathrm{sinc}(k_y a)$. Most of the energy of this function is contained in the first lobe, $k_y a < \pi$. This is why there is little energy outside the radiation circle for $\kappa a = \pi$ [Fig. 5(b)]. Thus, the energy content inside the radiation circle is a consequence of the pressure field inside the jet. Also, the phase speed of the content inside the radiation circle is supersonic relative to a laboratory reference frame. This energy content inside the radiation circle represents modes that propagate along the axis of the jet. The implication for flow decomposition into radiating and nonradiating components is that some acoustic components lie within the radiation circle as well [$\kappa^2 < (\omega/c)^2$].

From Eq. (12) and the definition of γ, it can be seen that for $k_x > \kappa/(1+M)$, we get an exponentially decaying response inside the jet. Physically, this represents a subsonically propagating wave inside the jet that leads to an evanescent wave. This explains why the spectrum decays for $k_x > \kappa/(1+M)$ for moderate to high frequencies. The decay can also be explained using ray theory, which predicts a shadow region in a wedge in the forward direction with half angle $\cos^{-1}[1/(1+M)]$ (Morse and Ingard, 1968). A point on the radiation circle determines the direction of sound radiation to the far field. The angle to the jet axis is given by $\cos^{-1}(k_x/\kappa)$ (Goldstein, 2005). Thus, the shadow region predicted by ray theory is in agreement with the region of decay on the radiation circle in Figs. 5(b)–6(d).

3. High frequencies

For very high frequencies, we see a combination of the radiation circle and an ellipse. At high frequencies, we would get several wavelengths inside the jet [$y < a$; compare with Fig. 6(b)]. If a is large (say, infinite), then the spectra would correspond to that of a point source in a uniformly moving medium, which is an ellipse. This is what we see in Fig. 5(d). The ringing is because of the finiteness of a, which, in the wavenumber domain, results in the convolution of the sinc function with the radiation ellipse.

III. DIVERGING JET

In order to consider the effect of three-dimensionality and divergence of a jet on the results presented in Sec. II, we seek the acoustic field radiating from a monopole source embedded in a diverging axisymmetric mean flow at $(z/a, r/a) = (3,0)$. The mean flow was obtained from the DNS of a Mach 0.84 and Re 7200 turbulent jet embedded in a co-flow of Mach 0.2. The full details of the DNS are available in Sandberg *et al.* (2012), and its sound field is analyzed in Sec. IV. The acoustic field was obtained by solving the linearized Euler equations.

Figures 7(a), 7(c), and 7(e) show the density field at frequencies of $\kappa a = 0.1\pi$, π, and 2π, respectively. We have not considered the high frequency case ($\kappa a = 10\pi$) as the low Reynolds number jet considered here emits negligible sound at such high frequencies. The notation, $\rho_{ka}(\mathbf{x}, t_0)$, describes a linear combination of the real and imaginary parts of the temporal Fourier transform of ρ at frequency ka, defined as

$$\rho_{ka}(\mathbf{x}, t_0) = \frac{1}{\pi}\left(\Gamma_r(\mathbf{x}, ka)\cos(\omega t_0) - \Gamma_i(\mathbf{x}, ka)\sin(\omega t_0)\right), \tag{19}$$

where $\Gamma = \Gamma_r + i\Gamma_i$ is the temporal Fourier transform of $\rho(\mathbf{x}, t)$. This allows one to follow the evolution of the density field at frequency ka with time. Figures 7(b), 7(d), and 7(f) show the corresponding wavenumber spectra. Comparing these figures for the case of monopole in the plug flow at the

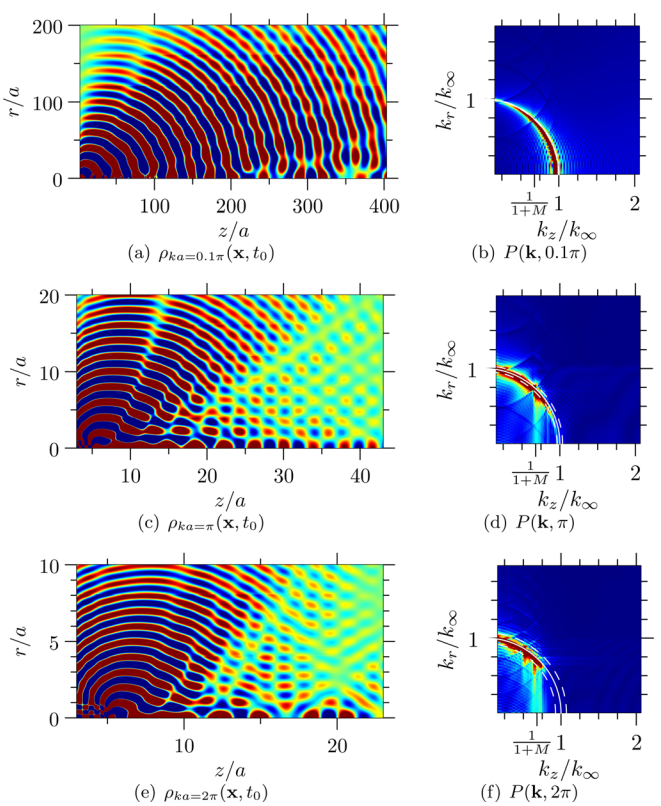

FIG. 7. (Color online) Density field radiating from a monopole in a diverging mean flow of a turbulent jet plotted in the physical domain (snapshot in left column) and wavenumber domain (magnitude of Fourier transform in right column) with color range $[-5\times10^{-5}, 5\times10^{-5}]$ and $[0, 0.15]$, respectively, for normalized frequencies $\kappa a/\pi = 0.1$, 1, and 2 and an arbitrary time, t_0 [cf. Eq. (19)]. In the right column, the arc shows the radiation circle, $|\mathbf{k}| = \omega/c_\infty$. The dashed arcs are at $|\mathbf{k}| = \omega/c_\infty \pm \Delta k/2$, where $\Delta k = \sqrt{\Delta k_z^2 + \Delta k_r^2}$ is the grid step in the wavenumber domain.

Redistribution subject to ASA license or copyright; see http://acousticalsociety.org/content/terms. Download to IP: 152.78.242.156 On: Wed, 17 Dec 2014 10:07:03

same frequencies [Figs. 5(a)–5(c)], we can see that the diverging jet has not changed the nature of the spectra. They look very similar. We see the radiation circle, the shadow region, and the vertical line around $k_x = \kappa/(1+M)$, which can again be identified as axial waves. These waves are clearly visible around the centerline in the physical domain [Figs. 7(c) and 7(e)]. The density along the axis of the jet is shown in Fig. 8. The decay rate is a polynomial of order <2.5 for all frequencies and not exponential. Thus, the axial modes propagate along the axis of the jet.

The presence of axial modes inside the radiation circle implies that the filter, $|\mathbf{k}| = |\omega|/c_\infty$ (Fig. 1), does not capture all the acoustic waves within the jet. To do so, one may use the condition $|\mathbf{k}| \leq |\omega|/c_\infty$ instead.

IV. TURBULENT JET

The density field from the DNS (Sandberg *et al.*, 2012) of a Mach 0.84 and Re 7200 turbulent jet embedded in a co-flow of Mach 0.2 is shown in Fig. 9(a) at a Strouhal number (based on the jet exit diameter and velocity) of 1.1. This corresponds to $\kappa a = 0.92\pi$.

The usual fast Fourier transform algorithm is inconvenient for computing the temporal Fourier transform, since it requires storing the complete time history of the three-dimensional density field. Here, Goertzel's (1958) algorithm was used, instead, as it consumes the time history one frame at a time. No special windowing, i.e., a rectangular window, was used to keep the main lobe as narrow as possible. However, a small amount of spectral leakage from low frequencies was observed, resulting in highly supersonic components ($|\mathbf{k}| \leq 0.6k_\infty$) appearing in the wavenumber plots. These supersonic components are unphysical and have been filtered out by means of a low-pass filter of the form

$$W_L(\mathbf{k}) = \frac{1}{2}\big(1 + \tanh\big((|\mathbf{k}| - k_0)/(\sigma k_\infty)\big)\big), \tag{20}$$

where $k_\infty = \omega/c_\infty$, $k_0/k_\infty = 0.6$, $\sigma = 0.1$.

Figure 9(b) shows the Fourier transform of the density field. The dashed lines indicate the grid resolution of the Fourier transform, which is greater than the physical resolution due to zero padding. The physical resolution is low ($a\Delta k = 0.42$) because the computational domain is small in the radial direction ($r \leq 7a$).

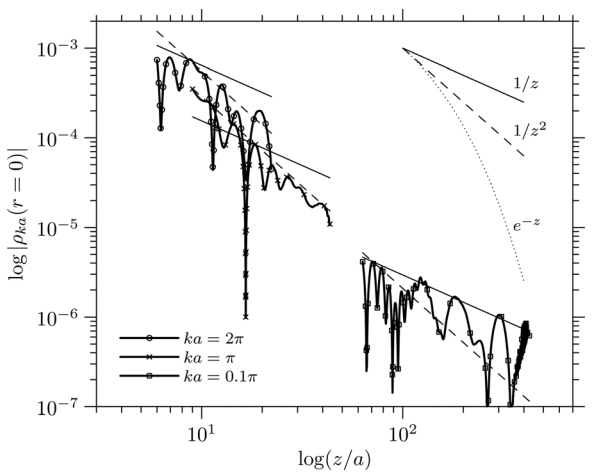

FIG. 8. Profiles of the density field and the associated decay rate along $r = 0$ for the data of Figs. 7(a), 7(c), and 7(e).

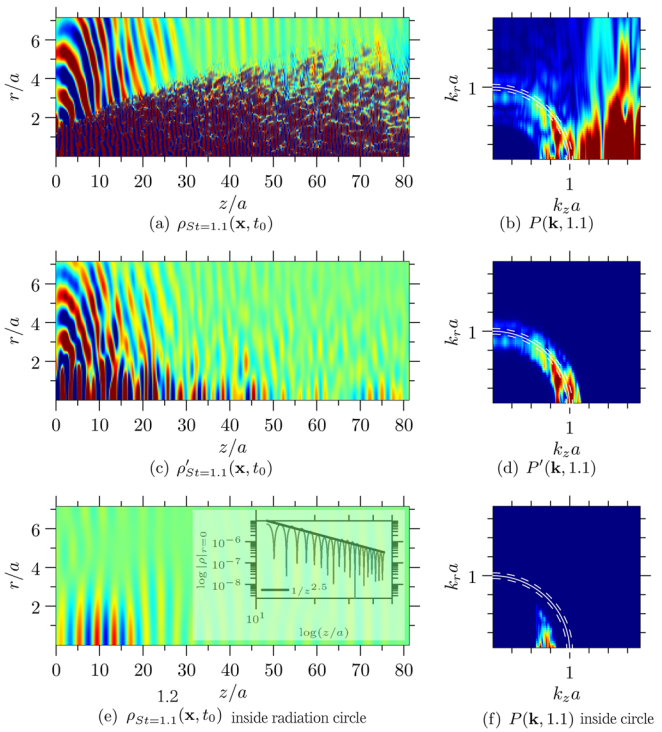

FIG. 9. (Color online) Density field in a turbulent jet plotted in the physical domain (snapshot in left column) and wavenumber domain (magnitude of Fourier transform in right column),with color range $[-8\times10^{-6}, 8\times10^{-6}]$ and $[0, 0.5]$, respectively, for a given normalized frequency, $St = 1.1$, and time, t_0 [cf. Eq. (19)]. The top row shows the density field, ρ, the middle row shows the radiating field based on the radiation circle, ρ', and the bottom row shows the part of the density field based on the inside of the radiation circle. In the right column, the arc shows the radiation circle, $|\mathbf{k}| = \omega/c_\infty$. The dashed arcs are at $|\mathbf{k}| = \omega/c_\infty \pm \Delta k/2$, where $\Delta k = \sqrt{\Delta k_z^2 + \Delta k_r^2}$ is the grid size in the wavenumber domain.

If we filter only along the radiation circle, as for the laminar jet, the density field in the Fourier domain and the corresponding field in the physical domain are shown in Figs. 9(d) and 9(c), respectively. A qualitative comparison between Figs. 9(a) and 9(c) shows that this filter, based on the radiation circle, captures most of the acoustic waves. But, it can be seen from Fig. 9(b) that there is a significant amount of energy inside the radiation circle. From the above analysis, we expect that this region of the spectrum should contribute to axial waves along the axis of the jet. Figure 9(f) shows the filtered spectra when only the interior of the radiation circle is considered. The corresponding density field in the physical domain is shown in Fig. 9(e). As expected, the waves propagate close to the axis of the jet. The inset of Fig. 9(e) shows the magnitude of the density field along the centerline of the jet. As in Sec. III, we get a polynomial decay rate for these axial waves.

Based on the above discussions, we can predict that if we are interested in the far field acoustic wave radiating at a particular angle, θ, then we can obtain this by filtering on the radiation circle in the frequency-wavenumber domain for the same polar angle in the $k_r - k_z$ plane. This is not surprising and was shown theoretically by Goldstein (2005). However,

Redistribution subject to ASA license or copyright; see http://acousticalsociety.org/content/terms. Download to IP: 152.78.242.156 On: Wed, 17 Dec 2014 10:07:03

for mid to high frequencies, this procedure would miss the effect of axial waves that propagate close to the axis of the jet.

It is worth noting that the wavenumber-frequency makeup of the acoustic spectra is different than that of the turbulence. The turbulent kinetic energy spectrum is generally obtained from numerical data by the application of the three-dimensional Fourier transform in space. The resulting spectrum contains a broad range of wavenumbers. For the low range of wavenumbers, corresponding to those that lie inside the radiation circle, one may think that there is no separation between the turbulence and acoustic spectra. This is not the case because the radiation circle is defined for a particular frequency; a Fourier transform in time is required in addition to the Fourier transform in space. In that case, for a given frequency, only a narrow band of wavenumbers make up the turbulent spectrum. In general, that narrow band would lie outside the radiation circle (corresponding to subsonic propagation speeds). For example, to compute the turbulence spectrum from experimental data, it is common practice to measure at a single point in space and to Fourier transform the signal in time. The Fourier transform in space is then obtained by invoking Taylor's hypothesis: assuming a frozen pattern of turbulence convected at a local flow speed, U, the wavenumber and frequency are related by $\omega/k = U$. Thus, for a given frequency, we are picking out a single wavenumber of the turbulence spectrum that corresponds to this dispersion relation. For a subsonic jet, this corresponds to a subsonic wave that lies outside the radiation circle. Thus, for the example problem considered here, the turbulence spectrum corresponds to the energy content to the right of the radiation circle in Fig. 9(b).

V. CONCLUSIONS

Most of the acoustic waves radiating from a jet satisfy the d'Alembertian dispersion relation, $k = \omega/c_\infty$, i.e., they lie on the radiation circle in the frequency-wavenumber domain. This is in agreement with the radiation sphere criterion proposed by Goldstein (2005) and used by Sinayoko *et al.* (2011). Note that the radiation sphere criterion was developed based on Lighthill's acoustic analogy. In order to derive the criterion, we have to treat the entire jet as a source region, that is, as a source term to the ordinary wave operator. Thus, the dispersion relation is d'Alembertian and wherever the wave equation is not satisfied, i.e., inside the jet, we get a source. Hence, this approach does not tell us what happens inside the source region—the jet.

At low Strouhal numbers (e.g., $\mathrm{St} \leq 0.5$), acoustic waves lie mainly on the radiation circle ($k = \omega/c_\infty$). This explains why the dispersion relation based on an ordinary wave equation was sufficient to filter out the acoustic waves even inside the jet, as shown in Fig. 2(c).

At mid-Strouhal numbers ($\mathrm{St} \sim 1$), some acoustic waves propagate along the axis of the jet. These waves can be classified as acoustic based on the observation that

(1) They propagate along the axis.

(2) They have supersonic phase speed $k < \omega/c_\infty$ (in a subsonic jet, the hydrodynamic waves and the energy associated with turbulent structures convect at subsonic speeds).

These axial waves could be identified by using the criterion $k \leq \omega/c_\infty$. Alternatively, one can use the axial wavenumber, $|k_x| \leq \omega/c_\infty$, since there are usually no hydrodynamic components such that $|k_x| < \omega/c_\infty$ and $|k_r| > \omega/c_\infty$. These would represent (unphysical) waves with axial wavelengths larger than acoustic waves traveling at subsonic speeds at high angles to the downstream jet axis. An advantage of this approach is that it does not require computing the radial Fourier transform.

Finally, at high Strouhal numbers ($\mathrm{St} \gg 1$), some acoustic waves lie around the radiation ellipse corresponding to the dispersion relation for waves propagating through a flow of Mach number equal to the average convection Mach number. These waves can, therefore, extend outside the radiation circle.

The above conclusions were shown to hold for sound propagation through a time-averaged diverging jet and a turbulent jet. Similar results could likely be obtained for other turbulent flows, such as mixing layers and wakes. If the flow field in the far field is non-quiescent, which could be the case for a mixing layer, then the radiation circle turns into a radiation ellipse.

Agarwal, A., Morris, P. J., and Mani, R. (**2004**). "Calculation of sound propagation in nonuniform flows: Suppression of instability waves," AIAA J. **42**(1), 80–88.

Cabana, M., Fortuné, V., and Jordan, P. (**2008**). "Identifying the radiating core of Lighthill's source term," Theor. Comput. Fluid Dyn. **22**(2), 87–106.

Cavalieri, A. V. G., Jordan, P., Colonius, T., and Gervais, Y. (**2012**). "Axisymmetric superdirectivity in subsonic jets," J. Fluid Mech. **704**, 388–420.

Chu, B.-T., and Kovasznay, L. S. G. (**1958**). "Non-linear interactions in a viscous heat-conducting compressible gas," J. Fluid Mech. **3**(5), 494–514.

Crighton, D. G. (**1985**). "The kutta condition in unsteady flow," Annu. Rev. Fluid Mech. **17**(1), 411–445.

Freund, J. B. (**2001**). "Noise sources in a low-Reynolds-number turbulent jet at Mach 0.9," J. Fluid Mech. **438**, 277–305.

Goertzel, G. (**1958**). "An algorithm for the evaluation of finite trigonometric series,"Am. Math. Monthly **65**(1), 34–35.

Goldstein, M. E. (**2005**). "On identifying the true sources of aerodynamic sound," J. Fluid Mech. **526**, 337–347.

Mani, R. (**1972**). "A moving source problem relevant to jet noise," J. Sound Vib. **25**(2), 337–347.

Morgan, J. D. (**1975**). "The interaction of sound with a subsonic cylindrical vortex layer," Proc. R. Soc. London, Ser. A **344**(1638), 341–362.

Morse, P. M., and Ingard, K. U. (**1968**). *Theoretical Acoustics* (Princeton University Press, Princeton, NJ), p. 713.

Obrist, D. (**2009**). "Directivity of acoustic emissions from wave packets to the far field," J. Fluid Mech. **640**, 165–186.

Sandberg, R. D., Suponitsky, V., and Sandham, N. D. (**2012**). "DNS of compressible pipe flow exiting into a coflow," Int. J. Heat Fluid Flow **35**, 33–44.

Sinayoko, S., and Agarwal, A. (**2012**). "The silent base flow and the sound sources in a laminar jet," J. Acoust. Soc. Am. **131**(3), 1959.

Sinayoko, S., Agarwal, A., and Hu, Z. (**2011**). "Flow decomposition and aerodynamic sound generation," J. Fluid Mech. **668**, 335–350.

Stromberg, J. L., McLaughlin, D. K., and Troutt, T. R. (**1980**). "Flow field and acoustic properties of a Mach number 0 9 jet at a low Reynolds number," J. Sound Vib. **72**(2), 159–176.

Tinney, C. E., and Jordan, P. (**2008**). "The near pressure field of co-axial subsonic jets," J. Fluid Mech. **611**, 175–204.

Redistribution subject to ASA license or copyright; see http://acousticalsociety.org/content/terms. Download to IP: 152.78.242.156 On: Wed, 17 Dec 2014 10:07:03